DOI: 10.1021/ma1006914

Macromolecules
ARTICLE

Glass (T_g) and Stimuli-Responsive (T_{SR}) Transitions in Random Copolymers

Fang Liu, William L. Jarrett, and Marek W. Urban*

Shelby F. Thames Polymer Science Research Center School of Polymers and High Performance Materials, The University of Southern Mississippi, Hattiesburg, Mississippi 39406

Received March 30, 2010; Revised Manuscript Received May 3, 2010

ABSTRACT: In an effort to elucidate the origin of stimuli-responsive (T_{SR}) transitions and correlate them to the glass transition temperature (T_g), poly(*N*-acryloyl-*N*′-propylpiperazine-*co*-2-ethoxyethyl methacrylate) (p(AcrNPP/EEMA)), poly(*N*-vinylcaprolactam-*co*-*n*-butyl acrylate) (p(VCl/nBA)), poly(*N*-isopropyl methacrylamide-*co*-*n*-butyl acrylate) (p(NIPMAm/nBA)), and poly(2-(*N,N*′-dimethylamino)ethyl methacrylate-*co*-*n*-butyl acrylate) (p(DMAEMA/nBA)) colloidal dispersions were synthesized, which upon coalescence form solid films. These studies showed that molecular rearrangements responsible for the T_{SR} transitions are attributed to the backbone buckling and collapse of stimuli-responsive components. Based on empirical data, the relationship between T_g and T_{SR} was established: $\log(V_1/V_2) = (P_1(T_{SR} - T_g))/(P_2 + (T_{SR} - T_g))$, where the V_1 and V_2 are the copolymer total volumes below and above the T_{SR}, respectively, T_g is the glass transition temperature of the copolymer, and P_1 and P_2 are the fraction of the free volume (f_{free}) at T_g (P_1) and $(T_{g,midpoint} - T_{SR})_{50/50}$) for each random copolymer (P_2), respectively. This relationship can be utilized to predict the total volume changes as a function of $T_{SR} - T_g$ for different copolymer compositions. To our best knowledge, this is the first study that provides the relationship between the T_{SR}, T_g, free volume, chain mobility, and dimensional changes in stimuli-responsive random copolymer networks.

Introduction

While the design and synthesis of stimuli-responsive polymeric materials to achieve orchestrated and orderly responsive networks continue to be a challenge,[1−6] limited efforts have been made to understand physicochemical aspects of stimuli-responsiveness, in particular, solid networks. As pointed out earlier,[7,8] polymeric solutions, surfaces and interfaces, and to a certain degree polymer gels facilitate energetically and spatially favorable environments for stimuli-responsiveness. The main challenge is, however, to design solid polymer networks that sustain their useful functionalities while being stimuli-responsive.[7,8]

Since spatial and energetic network attributes are influenced by chemical and morphological network features, recent studies[9−11] have shown that the presence of localized "voids" is one of the prerequisites for segmental rearrangements, which is facilitated by the presence of a low glass transition (T_g) copolymerized component. Following this concept, poly(*N*-DL-(1-hydroxymethyl)propylmethacrylamide-*co*-*n*-butyl acrylate) (p(DL-HMPMA/nBA))[11] and poly(2-(*N,N*′-dimethylamino)ethyl methacrylate-*co*-*n*-butyl acrylate) (p(DMAEMA/nBA))[10] copolymer films with thermal-sensitive attributes were prepared, whereby by the presence of temperature-responsive DL-HMPMA and DMAEMA units result in dimensional changes above and below stimuli-responsive transitions (T_{SR}).[9] These endothermic relaxations occur above the T_g, whereas the low-T_g nBA provids free volume for spatial rearrangements. Since at T_g the kinetic energy of the segmental motions results from the access of free volumes above the T_g,[12−14] the T_{SR} transitions were related to the compositional changes.

In view of these considerations, one needs to raise the question if the T_g and T_{SR} transitions are significant and, if so, how are they related to each other. Qualitatively, the presence of the T_g with the respect to the environment determines the functionality of polymeric materials that is related to properties via the WLF equation. In this context, the presence of the T_{SR} in stimuli-responsive polymers will also reflect mobility and conformational and structural features. Thus, free volume changes as a function of temperature will be affected by not only the T_g but also the T_{SR}. These studies will elucidate the origin of T_{SR} transitions and their relationship to the T_g, free volume, and dimensional changes in stimuli-responsive solid films of poly(*N*-acryloyl-*N*′-propylpiperazine-*co*-2-ethoxyethyl methacrylate) (p(AcrNPP/EEMA)), poly(*N*-vinylcaprolactam-*co*-*n*-butyl acrylate) (p(VCl/nBA)), poly(*N*-isopropylmethacrylamide-*co*-*n*-butyl acrylate) (p(NIPMAm/nBA)), and poly(2-(*N,N*′-dimethylamino)ethyl methacrylate-*co*-*n*-butyl acrylate) (p(DMAEMA/nBA)). For the purpose of these studies, these colloidal particles were synthesized and coalesced to form uniform films, in which volume changes were induced by temperature.

Experimental Section

N-Acryloyl-*N*′-propylpiperazine (AcrNPP) (99%) was purchased from Eastern Systems, Inc. Hexadecyltrimethylammonium chloride (HTAc) solution (25 wt % in H_2O) was purchased from Fluka Chemical Co. *N*-vinylcaprolactam (VCl) (98%) and 2-(*N,N*′-dimethylamino)ethyl methacrylate (DMAEMA) (97%) were purchased from Polysciences Inc. 2,2′-Azobis(isobutyronitrile) (AIBN) (98%), potassium persulfate (KPS) (99%), 2-ethoxyethyl methacrylate (EEMA) (99%), *n*-butyl acrylate (nBA) (99%), and *N*-isopropylmethacrylamide (NIPMAm) (97%) were purchased from Aldrich Chemical Co.

P(AcrNPP/EEMA), p(VCl/nBA), and p(DMAEMA/nBA) copolymers were synthesized using the semicontinuous emulsion polymerization process outlined elsewhere[15] which was adapted for a small-scale polymerization. The reaction flask was immersed in a water bath preheated to 75 °C and purged continuously with N_2 gas. The reactor was first charged with 27 mL of double deionized (DDI) water, and after purging N_2 for 30 min, the content was stirred at 350 rpm. At this point, pre-emulsion

*To whom correspondence should be addressed.

 Published on Web 05/18/2010

(DDI, 25 mL; HTAc, 0.62 g; weight-rationed monomers, 5.6 g; and oil-soluble initiator AIBN, 0.1 g) was fed at 0.156 mL/min into the vessel over a period of 3 h. After completion of pre-emulsion feeding, the reaction was continued for extra 3 h. The resulting colloidal dispersion was filtered after cooling to ambient temperature. For p(NIPMAm/nBA), 54 mL of DDI and 0.62 g of HTAc surfactant solution were first transferred into a 100 L reaction flask which equipped with a reflux condenser in a 75 °C water bath under the N_2 atmosphere and stirred at 350 rpm for 30 min. At this point, 5.6 g of NIPMAm/nBA monomers was added to prepare the pre-emulsion. Then 10.1 mL of a 3.6×10^{-2} M solution of KPS and DDI H_2O was fed into the reaction kettle for 3 h, followed by further reaction for an additional 3 h and subsequent cooling to room temperature. The pH values of these resulting original colloidal dispersions are ~8.5 determined by potentiometric titration.

Molecular weight was determined using gel permeation chromatography (Waters, Inc.) equipped with a 515 HPLC pump and a 2414 model refractive index detector. Each sample was precipitated in tetrahydrofuran (THF) and eluted through a 5 μm MIXED-C column. Elution times were referenced against polystyrene standards, and molecular weights of the copolymers were within $(1.33-2.15) \times 10^5$ g/mol.

Polymeric films were prepared by casting colloidal dispersions onto a poly(tetrafluoroethylene) (PTFE) substrate and allowed to coalescence at 45% relative humidity (RH) for 72 h at 22 °C in an environmental chamber. In a typical experiment, ~200 μm thick films were obtained and 15 × 10 mm sections were used for dimensional change experiments. Each specimen was equilibrated for 4 h at a given temperature before measuring the dimensional changes using a micrometer (Mitutoyo Co.) with a precision of ±0.1 μm.

Differential scanning calorimetry (DSC) measurements were performed on a TA Instruments DSC Q 100 under a N_2 atmosphere. Multiple DSC thermal cycles were conducted using the following heating−cooling schedule: the specimen was equilibrated at −50 °C for 5 min, followed by heating at 3 °C/min to 70 °C, equilibrating at 70 °C for 5 min, and cooling down at 3 °C/min to −50 °C. The same cycle was repeated several times. The resulting data were analyzed using TA Universal Analysis software.

Microscopic attenuated total reflectance Fourier transform infrared (ATR FT-IR) spectra were collected on a Bio-Rad FTS-6000 FT-IR single-beam spectrometer set at 4 cm^{-1} resolution equipped with a deuterated triglycine sulfate (DTGS) detector. A 2 mm Ge crystal with a 45° face angle maintaining constant contact pressure between the crystal and the specimens was used. Each spectrum was collected on the film interface with attached heating elements and represented 100 coadded scans ratioed to 100 scans collected on an empty ATR cell. All spectra were corrected for spectral distortions by Q-ATR software using the Urban−Huang algorithm.[16]

Raman spectra were obtained using a Renishaw inVia Raman microscope equipped with a computer-controlled three-axis encoded (X, Y, Z) motorized stage, a RenCam CCD detector, and a Leica microscope (DMLM series). The 785 nm diode laser provided an excitation source with a maximum power output of 300 mW. The films were placed on the gold surface, and each Raman spectrum was collected at a 100 mW laser power and an acquisition time of 45 s.

Solid-state ^{13}C NMR spectra were acquired using a UNITY INOVA 400 spectrometer equipped with a Chemagnetics 7.5 mm two-channel solids probe. The samples were spun at a rate of 4.0 kHz. The ^1H 90° pulse duration was 5.5 μs, and the acquisition time was 45 ms. A proton decoupling field strength of 52 kHz was used to remove $^{13}C-^1H$ dipolar broadening. The free induction decays (FIDs) were zero-filled to 32 K data points, and Lorentzian and Gaussian apodization was applied prior to Fourier transformation.

Quantum mechanical semiempirical calculations were conducted using Material Studio software (Accelrys Inc., Version 4.1). Computer modeling simulations were performed with the COMPASS

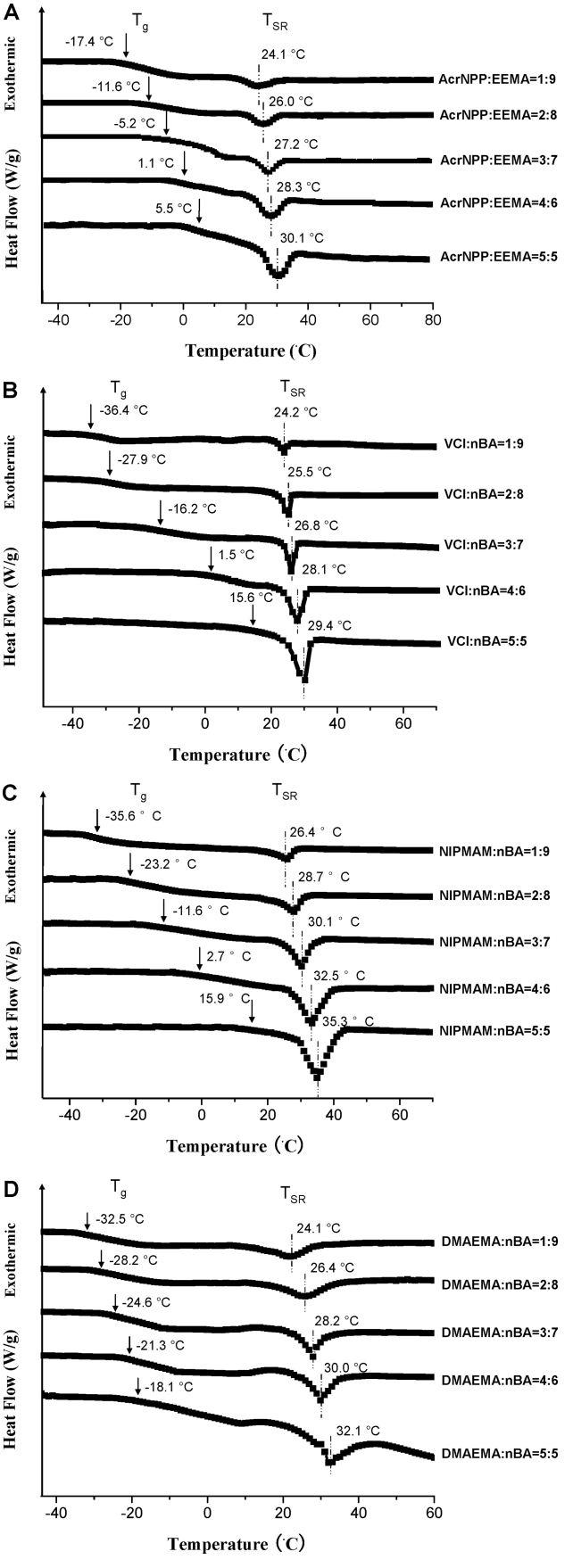

Figure 1. Series DSC thermograms of (A) p(AcrNPP/EEMA), (B) p(VCl/nBA), (C) p(NIPMAm/nBA), and (D) p(DMAEMA/nBA) recorded as a function of copolymer composition.

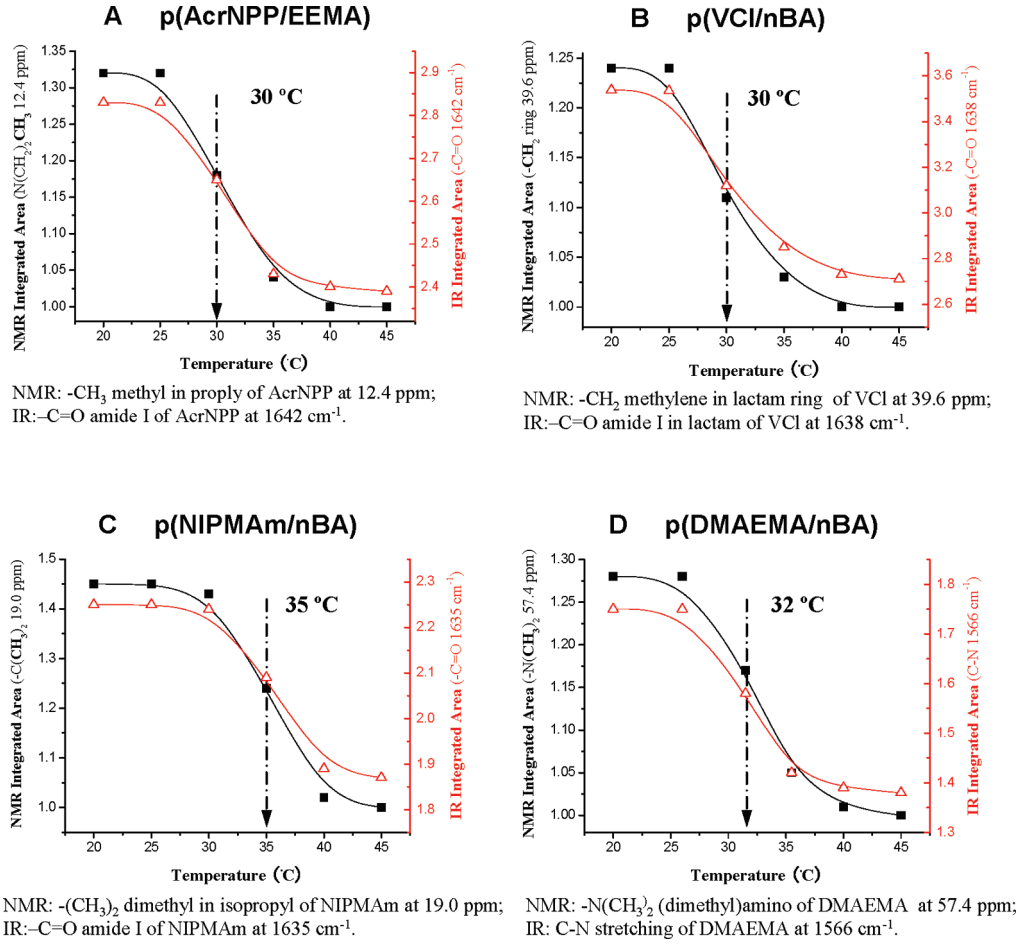

NMR: -CH_3 methyl in proply of AcrNPP at 12.4 ppm; IR:–C=O amide I of AcrNPP at 1642 cm^{-1}.

NMR: -CH_2 methylene in lactam ring of VCl at 39.6 ppm; IR:–C=O amide I in lactam of VCl at 1638 cm^{-1}.

NMR: -$(CH_3)_2$ dimethyl in isopropyl of NIPMAm at 19.0 ppm; IR:–C=O amide I of NIPMAm at 1635 cm^{-1}.

NMR: -$N(CH_3)_2$ (dimethyl)amino of DMAEMA at 57.4 ppm; IR: C-N stretching of DMAEMA at 1566 cm^{-1}.

Figure 2. Integrated area of NMR (■) resonance and IR (Δ) bands of (A) p(AcrNPP/EEMA), with NMR resonance of −CH_3 in propyl group of AcrNPP at 12.4 ppm, and IR band of −C═O amide I of AcrNPP at 1642 cm^{-1}. (B) p(VCl/nBA), with NMR resonance of −CH_2 in lactam ring of VCl at 39.6 ppm and IR band of −C═O lactam amide I of VCl at 1638 cm^{-1}. (C) p(NIPMAm/nBA), with NMR resonance of −$(CH_3)_2$ in isopropyl group of NIPMAm at 19.0 ppm and IR band of −C═O amide I of NIPMAm at 1635 cm^{-1}. (D) p(DMAEMA/nBA), with NMR resonance of −$N(CH_3)_2$ (dimethyl)amino of DMAEMA at 57.4 ppm and IR band of −C−N stretch of DMAEMA at 1566 cm^{-1} plotted as a function of temperature for 50/50 copolymer ratio.

force field conditions. In the first step, we created infinite random polymer long chains using 3D periodic boundary conditions. In an effort to determine thermodynamic responses of polymer segments, a periodic unit cell containing five polymer chains was constructed, and temperature was the control parameter to simulate the heat exchange with the environment. This method involves computing *NVT* (constant number, volume, and temperature) molecular dynamics at a set temperature using 25 000 steps and 25 ps (ps) (dynamic times), followed by another *NPT* (constant number, pressure, and temperature) molecular dynamics with 50 000 steps and dynamic times 50 ps, and then *NVE* (constant number, volume, and energy) molecular dynamics with 100 000 steps and 100 ps. The purpose of this three-step process is to simulate energy, volume, and conformational changes at different temperatures.

Results and Discussion

While the Supporting Information provides detailed chemical, structural, and compositional analysis of p(AcrNPP/EEMA), p(VCl/nBA), p(NIPMAm/nBA), and p(DMAEMA/nBA) copolymers after copolymerization, Figure 1A−D illustrates a series of DSC thermograms as a function of the copolymer composition of these copolymer films, respectively. As seen, two composition-dependent endothermic transitions T_g and T_{SR} are detected, which shift to higher temperatures as the w/w fraction of the stimuli-responsive component increases. As anticipated, the energy required for the T_{SR} transitions to occur increases proportionally to the amount of stimuli-responsive components incorporated into the copolymer backbone. Also, the T_{SR} for p(DMAEMA/nBA) is significantly above the T_g compared to p(AcrNPP/EEMA), p(VCl/nBA), and p(NIPMAm/nBA) copolymers, indicating greater free volume and enhanced chain mobility available for DMAEMA/nBA network rearrangements. The DSC thermograms also show that, while the T_g transition appears as an expected change of thermal conductivity, the T_{SR} transition is an endothermic peak, which upon completion retains the same heat conductivity.

In order to determine which molecular entities are responsible for the T_{SR} endotherm, ATR FT-IR, Raman, and ^{13}C NMR measurements were performed as a function of temperature. While spectroscopic results are provided in the Supporting Information, Figure 2A−D illustrates integrated areas of the selected NMR resonances and IR bands plotted as a function of temperature. As seen, all curves decrease gradually as the temperature increases, with the middle point transitions at 30, 30, 35, and 32 °C for p(AcrNPP/EEMA), p(VCl/nBA), p(NIPMAm/nBA), and p(DMAEMA/nBA), respectively. These data are in good agreement with the T_{SR} transition minimum detected in the DSC measurements shown in Figure 1. Analysis of the spectroscopic data also indicate that, in addition to the C−H stretching vibrations due to backbone/side groups, amide and propylpiperazine functional groups of AcrNPP, amide and lactam ring vibrations of VCl, isopropyl and amide linkages of NIPMAm, and (dimethylamino)ethyl functional groups of DMAEMA are also sensitive to the T_{SR} transitions in each copolymer.

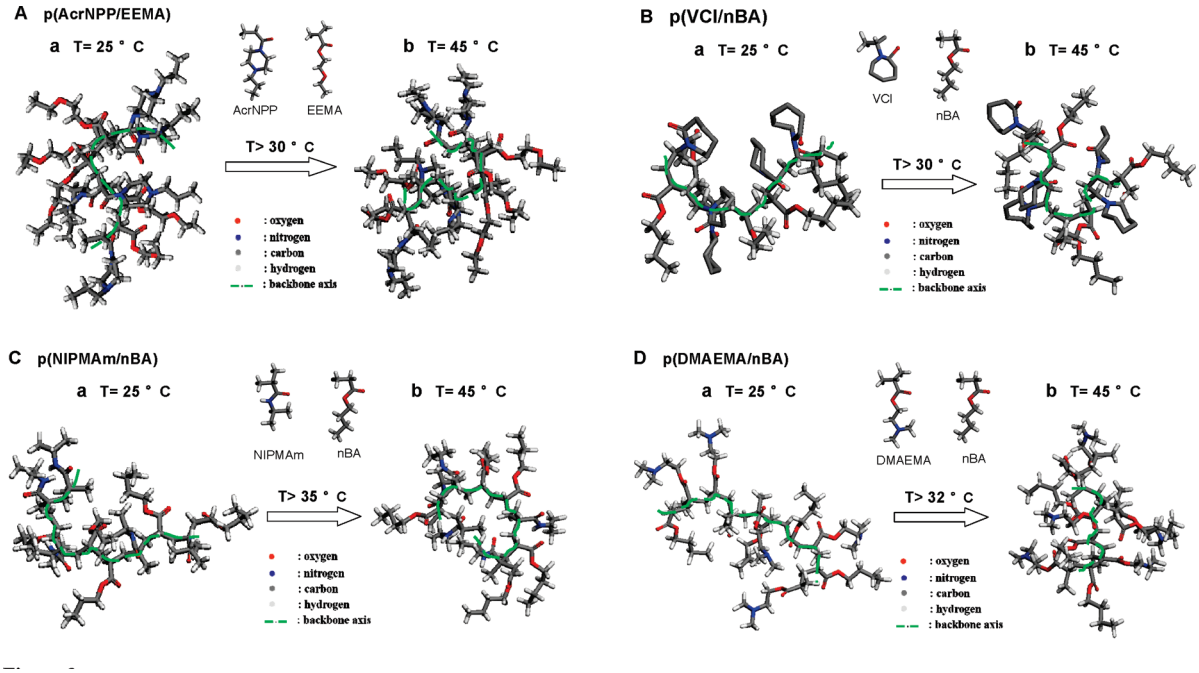

Figure 3. Results of computer simulations representing molecular conformation changes at 25 °C (a) and 45 °C (b) of copolymers (A) p(AcrNPP/EEMA), (B) p(VCl/nBA), (C) p(NIPMAm/nBA), and (D) p(DMAEMA/nBA).

To further elucidate the origin of molecular changes responsible for the T_{SR} transitions, thermodynamic computer simulations were performed, in which infinite copolymer chains were constructed by randomly connecting energy minimized monomer units under 3D periodic boundary conditions. While the Experimental Section provides computational details, visualization of the results is illustrated in Figure 3A−D. As seen, when going from 25 to 45 °C, the copolymer backbones buckle up and the stimuli-responsive components collapse at 45 °C (above T_{SR}), which is caused by conformational changes.[10] The calculated total energies (ΔE_{tot}) for the T_{SR} transition of p(AcrNPP/EEMA), p(VCl/nBA), p(NIPMAm/nBA), and p(DMAEMA/nBA) are 132, 127, 176, and 223 kcal/mol, respectively, whereas the endothermic transition energies (enthalpy) detected in DSC are 93, 90, 145, and 189 kcal/mol. While the observed trends are in agreement with the energy values obtained from the theoretical measurements, ~40 kcal/mol difference is attributed to the entropic component incorporated in the ΔE_{tot} calculations, but not measured by DSC. The above analysis indicate that molecular rearrangements at the T_{SR} result in the collapse of stimuli-responsive side chains and buckling of the backbone, which is also reflected in dimensional changes leading to the volume shrinkage.[10,11]

In order to relate the T_{SR} to polymer chain mobility, free volume, T_g, and dimensional changes, $\log(V_1/V_2)$ was plotted as a function of $(T_{SR} - T_g)$. The results are illustrated in Figure 4A−D for p(AcrNPP/EEMA), p(VCl/nBA), p(NIPMAm/nBA), and p(DMAEMA/nBA), respectively, where the solid cubic (■) points represent the DSC experimental data points plotted for different compositions and the solid lines represent the best curve fitting. As seen, the greater total volume changes are detected for copolymer compositions with a higher content of stimuli-responsive components (smaller $T_{SR} - T_g$ values). As the $T_{SR} - T_g$ value increases (less stimuli-responsive component is incorporated into a copolymer backbone), the changes of total volume decrease nonlinearly. Compared to other copolymers, p(DMAEMA/nBA) copolymer (Figure 4D) exhibits the greater total volume changes for each composition attributed to the higher free volume, and thus enhanced chain mobility as the T_{SR} is further away from the T_g for all p(DMAEMA/nBA) copolymer compositions. It should be noted that the DSC experimental points are discrete with the best logarithmic hyperbolic curve fitting (the red curves).

The empirical relationship predicting the total volume changes as a function of the $(T_{SR} - T_g)$ for different copolymer compositions with the calculated P_1 and P_2 values for each copolymer (assuming that the contributions of free volume to total volume changes above the T_g are neglectable[17]) can be expressed as

$$\log \frac{V_1}{V_2} = \frac{P_1(T_{SR} - T_g)}{P_2 + (T_{SR} - T_g)} \quad (1)$$

where V_1 is the copolymer total volume below T_{SR}, V_2 is the copolymer total volume above T_{SR}, T_{SR} is the stimuli-responsive transition temperature, and T_g is the glass transition temperature of the copolymer. The calculated P_1 values correspond to the fraction of the free volume (f_{free}) at T_g,[18] and based on the free volume theory,[17,19−21] the reported f_{free} values for various polymers are in the 0.013−0.113 range. The calculated P_1 values for p(AcrNPP/EEMA), p(VCl/nBA), p(NIPMAm/nBA), and p(DMAEMA/nBA) are 0.032, 0.042, 0.053, and 0.016, respectively. It is therefore reasonable to assume that $P_1 \approx f_{free}$. On the other hand, the calculated P_2 values can be approximated to the temperature difference between the $T_{g,midpoint}$ and T_{SR} ($(T_{g,midpoint} - T_{SR})_{50/50}$) for random copolymers with the 50/50 ratio. As the copolymer networks shrink at the T_{SR}, the copolymer density will change ($M = \rho V$, where M is the total mass, ρ is the density, and V is the total volume.). Upon substitution, eq 1 will become

$$\log \frac{\rho_b}{\rho_a} = \frac{P_1(T_{SR} - T_g)}{P_2 + (T_{SR} - T_g)} \quad (2)$$

where ρ_a and ρ_b are the copolymer densities below and above the T_{SR}. Using eq 2, one can predict the density changes as a function of the $(T_{SR} - T_g)$ for different copolymer compositions. For example, the relative density ratios below and above the T_{SR} are

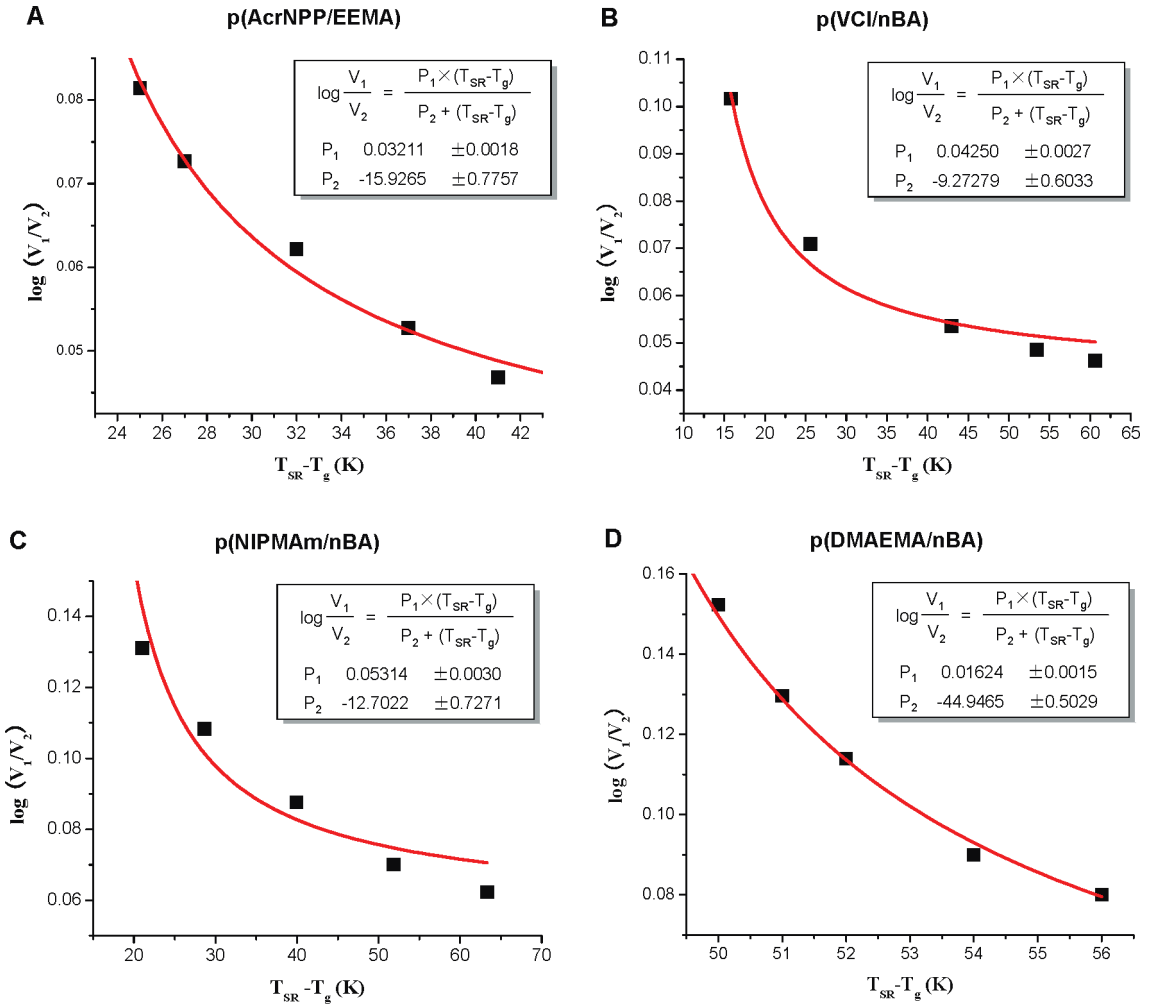

Figure 4. Curve fitting of the experimental T_{SR} values obtained from DSC measurements using eq 1: (A) p(AcrNPP/EEMA), (B) p(VCl/nBA), (C) p(NIPMAm/nBA), and (D) p(DMAEMA/nBA).

ρ_b/ρ_a = 1.23, 1.28, 1.38, and 1.42 for p(AcrNPP/EEMA), p(VCl/nBA), p(NIPMAm/nBA), and p(DMAEMA/nBA) (at 50/50 ratio). These predictions are in a good agreement with the experimental macroscopic changes (V_1/V_2) at T_{SR}, which are 1.2, 1.27, 1.34, and 1.41, respectively.

It should be noted that the calculated P_1 and P_2 values for these copolymers are not universal constants. We determined their values for all compositions examined in this study, and as an example justifying their physical significance, the P_1 and P_2 values were plotted for a 50/50 copolymer composition as a function of the ($T_{SR} - T_g$). The results are illustrated in Figure S9 of the Supporting Information and illustrate that the P_1 values of p(AcrNPP/EEMA), p(VCl/nBA), and p(NIPMAm/nBA) are located in the 0.032−0.055 window, whereas the P_1 value of p(DMAEMA/nBA) is at 0.016. The same features are observed for the P_2 which fall in the −15 to −9 window for p(AcrNPP/EEMA), p(VCl/nBA), and p(NIPMAm/nBA), but for p(DMAEMA/nBA) is −45. This analysis indicates that P_1 and P_2 are not universal constants, and more importantly, their magnitude depends upon the free volume available for chain rearrangements. For example, as we recall the DSC data shown in Figure 1 for p(DMAEMA/nBA) copolymer, the T_{SR} is significantly above the T_g compared to other copolymers, thus exhibiting greater free volume and higher chain mobility. This is attributed to structural similarities between p(AcrNPP/EEMA), p(VCl/nBA), and p(NIPMAm/nBA) with the presence of amide linkages and ester groups in p(DMAEMA/nBA). It has been reported[22−25] that the C_1 and C_2 constants in the WLF equation also vary significantly for the various homo- and copolymers. However, the P_1 and P_2 in eq 1 fall into specific ranges, depending upon the $T_{SR} - T_g$ difference. For the random copolymers, where $T_{SR} - T_g < 25$, the average P_1 and P_2 values are ∼0.045 and −12, whereas for $T_{SR} - T_g > 50$ (such as p(DMAEMA/nBA)), the P_1 and P_2 are ∼0.016 and −45.

To visualize the relationship between the volume and temperature changes and assuming that the total volume (V_{total}) of a copolymer is the sum of the free volume (V_{free}) and the volume occupied by polymer chains (V_{occupy}), Figure 5A,B was constructed and illustrates the temperature dependence of the V_{total}, V_{free}, and V_{occupy} for $T_{SR} > T_g$ and $T_{SR} \gg T_g$. As seen, below the T_g, the V_{free} remains almost constant, which significantly limits molecular mobility, thus allowing only small-scale localized side groups vibrations/rotations. At $T > T_g$, the V_{free} increases faster, thus mobilizing long-range segmental motions, and at T_{SR}, buckling of a copolymer backbone as well as the collapse of stimuli-responsive components occurs. As a result, the V_{total} will decrease, at the expense of V_{occupy} and/or V_{free}. This process, however, will compete with the V_{free} increase at above T_g. This is specially pronounced when $T_{SR} \gg T_g$ for p(DMAEMA/nBA) copolymers shown in Figure 5B. As seen, compared to the $T_{SR} > T_g$ (Figure 5A), the V_{free} significantly increases, activating long-range molecular motions and providing sufficient space for rearrangements and mobility of chains. As a result, conformation changes and shrinking at the T_{SR} occur, leading to larger

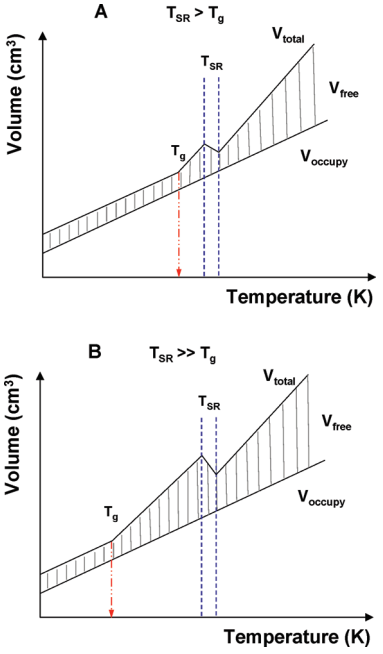

Figure 5. Schematic representation of the volume changes as a function of temperature for $T_{SR} > T_g$ (A) and $T_{SR} \gg T_g$ (B).

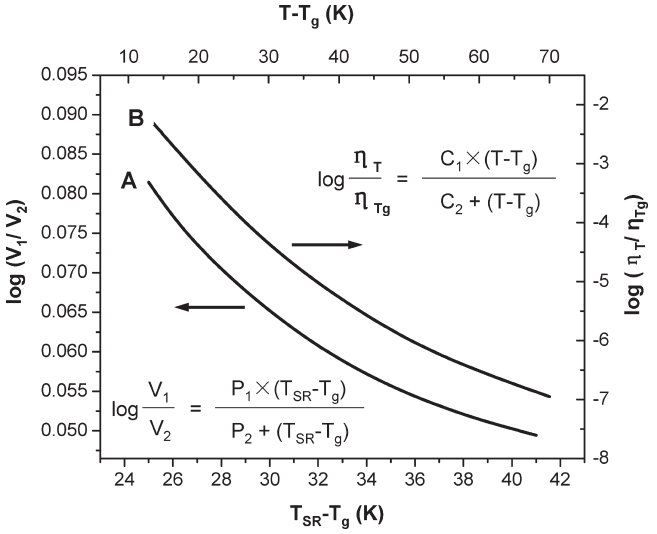

Figure 6. $\log(V_1/V_2)$ (A) and $\log(\eta_T/\eta_{T_g})$ (B) plotted as a function of $T_{SR} - T_g$ and $T - T_g$.

V_{total} decrease. Corresponding larger density changes are also anticipated, as predicted by eq 2. The coexistence of these competing processes is also reflected in thermally induced molecular interactions manifested as an exothermic transition immediately before the T_{SR}, which is illustrated in the DSC measurements in Figure 1D. As the copolymer temperature increases above the T_{SR}, the V_{free} and the polymer chain mobility are further enhanced, ultimately leading to the melt and flow of the entire polymer.

Since the T_g and T_{SR} are composition-dependent, let us go back to eq 1 and compare it with the WLF equation.[19] While the latter examines thermally dependent viscosity changes[19,26] in polymer liquid/melts, eq 1 relates molecular relaxations and V_{total} changes when T_{SR} transitions are present. Also, the WLF equation is applicable for linear polymers within $T_g - T_g + 100$ temperature range, whereas eq 1 can be utilized for stimuli-responsive random or alternative copolymers within the $T_{SR} - T_g$

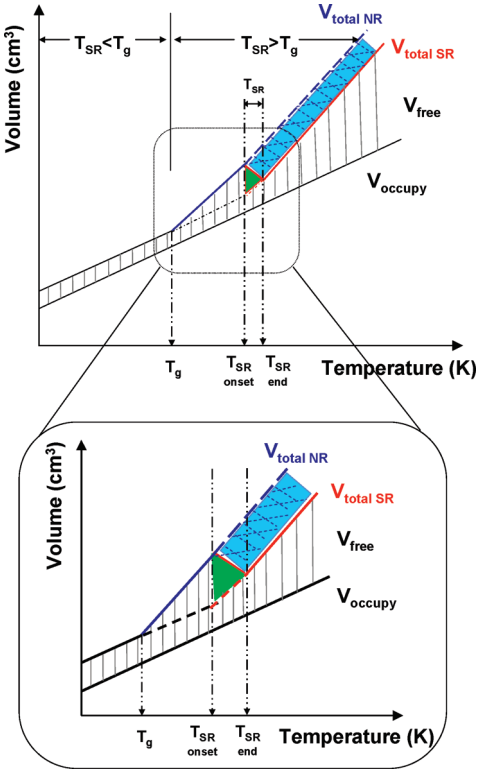

Figure 7. Schematic representation of the volume changes as a function of temperature for nonresponsive and stimuli-responsive polymers.

range. Since T_g and T_{SR} related η and V, respectively, Figure 6 was constructed in an effort to theoretically compare both relationships. As seen, curve A represents the $\log(V_1/V_2)$ changes as a function of $T_{SR} - T_g$, whereas curve B relates $\log(\eta_T/\eta_{T_g})$ and $T - T_g$. When the temperature difference ($T_{SR} - T_g$ and $T - T_g$) increases, both curves exhibit parallel declining trends, although, as anticipated, their magnitudes are quite different.

Finally, to compare the total volume changes as a function of temperature for nonresponsive ($V_{total\,NR}$) and stimuli-responsive ($V_{total\,SR}$) polymers, Figure 7 was constructed in which the $V_{total\,NR}$ (blue dashed line) continues to increase gradually, followed by an upward change above the T_g. For stimuli-responsive polymers (red line), the $V_{total\,SR}$ decreases at the T_{SR} due to the collapse of stimuli-responsive components and backbone buckling, followed by a further increase at the same rate (slope) due to retention of the heat capacity before and above the T_{SR} transition. The blue area corresponds to the $V_{total\,NR} - V_{total\,SR}$, while the green area represents the V_{free} required for stimuli-responsiveness to occur at T_{SR}. For a given polymer system, the lower T_g will provide more free volume at a given temperature, and when $T_{SR} < T_g$, the T_{SR} transition may not be present. For example, when replacing the low-T_g component (nBA or EEMA) by high-T_g MMA, with the $T_{g,p(MMA)}$ of 105 °C,[33] the diminished V_{free} will significantly affect copolymer thermal relaxations. This is theoretically illustrated in Figure 8, which shows that the T_g values of high T_g containing copolymer will be above the T_{SR} line for all compositions (Figure 8A−C), or only a small composition range is available for the T_{SR} transitions (Figure 8D). However, for low-T_g (nBA or EEMA) copolymers, the T_g values will be significantly lower, which consequently will interset with the T_{SR} line (Figure 8A−C) or will even be below (Figure 8D). As a result, significant composition variations (shaded area) are available for the T_{SR} to occur. Thus, regardless of the composition, the primary requirement to achieving the T_{SR} transitions in solid networks is that $T_{SR} > T_g$.

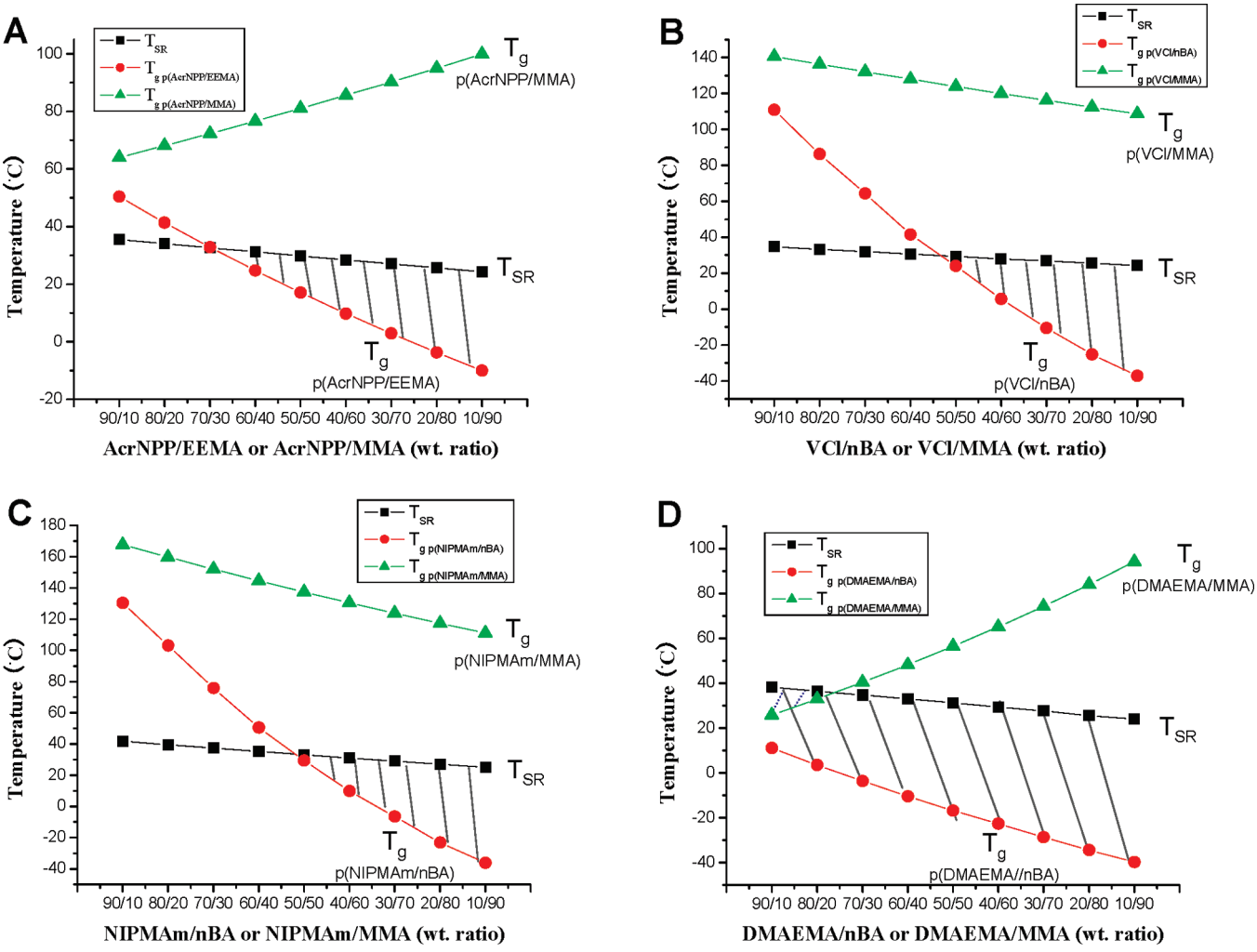

Figure 8. T_g and T_{SR} values plotted as a function of copolymer composition for AcrNPP (A), VCl (B), NIPMAm (C), and DMAEMA (D).

Conclusions

Stimuli-responsive p(AcrNPP/EEMA), p(VCl/nBA), p(NIPMAm/nBA), and p(DMAEMA/nBA) solid networks were prepared which exhibit two composition-dependent endothermic transitions, T_g and T_{SR}. Spectroscopic analyses combined with molecular simulations indicated the collapse of stimuli-responsive components and buckling of copolymer backbone are responsible for the T_{SR} transitions. Based on the experimental results, the empirical relationship $\log(V_1/V_2) = (P_1(T_{SR} - T_g))/(P_2 + (T_{SR} - T_g))$ was established which can be utilized to predict the total volume changes as a function of $T_{SR} - T_g$ for different copolymer compositions. Depending upon available free volume, the $P_1 = 0.045$ and $P_2 = -12$ are applicable for the majority of thermal-responsive components, whereas low-T_g temperature-sensitive components exhibit $P_1 = 0.045$ and $P_2 = -12$. Regardless of the solid-state composition of the stimuli-responsive network, the designed T_{SR} should be above the T_g in order to achieve sufficient free volume and chain mobility facilitating chain rearrangements at T_{SR}.

Acknowledgment. This work was primarily supported by the MRSEC Program of the National Science Foundation under Award DMR 0213883.

Supporting Information Available: Detailed chemical, structural, and compositional analysis of p(AcrNPP/EEMA), p(VCl/nBA), p(NIPMAm/nBA), and p(DMAEMA/nBA) copolymers after copolymerization. This material is available free of charge via the Internet at http://pubs.acs.org.

References and Notes

(1) Ghosh, B.; Urban, M. W. *Science* **2009**, *323*, 1458.
(2) Corten, C. C.; Urban, M. W. *Adv. Mater.* **2009**, *21*, 5011.
(3) Tokarev, I.; Minko, S. *Adv. Mater.* **2009**, *21*, 241.
(4) Morimoto, N.; Qiu, X. P.; Winnik, F. M. *Macromolecules* **2008**, *41*, 5985.
(5) Jonas, A. M.; Glinel, K.; Oren, R.; Nysten, B.; Huck, W. T. S. *Macromolecules* **2007**, *40*, 4403.
(6) Dong, D.; Lindau, M.; Ober, C. K. *Langmuir* **2009**, *25*, 4774.
(7) Liu, F.; Urban, M. W. *Prog. Polym. Sci.* **2010**, *35*, 3.
(8) Urban, M. W. *Prog. Polym. Sci.* **2009**, *34*, 679.
(9) Liu, F.; Urban, M. W. *Macromolecules* **2009**, *42*, 2161.
(10) Liu, F.; Urban, M. W. *Macromolecules* **2008**, *41*, 6531.
(11) Liu, F.; Urban, M. W. *Macromolecules* **2008**, *41*, 352.
(12) Boyer, R. F. *J. Appl. Phys.* **1954**, *25*, 825.
(13) Franck, A. *Macromol. Chem. Phys.* **1979**, *180*, 581.
(14) Chow, T. S. *Polym. Eng. Sci.* **1984**, *24*, 1079.
(15) Lestage, D.; Urban, M. W. *Langmuir* **2005**, *21*, 2150.
(16) Urban, M. W. *Attenuated Total Reflectance Spectroscopy of Polymers. Theory and Practice*; Washington, DC, 1989.
(17) Simha, R.; Boyer, R. F. *J. Chem. Phys.* **1962**, *37*, 1003.
(18) Fox, T. G.; Flory, P. J. *J. Appl. Phys.* **1950**, *21*, 581.
(19) Williams, M. L.; Landel, R. F.; Ferry, J. D. *J. Am. Chem. Soc.* **1955**, *77*, 3701.
(20) Simha, R.; Weil, C. E. *J. Macromol. Sci., Phys.* **1970**, *B4*, 215.
(21) Boyer, R. F.; Simha, R. *J. Polym. Sci.* **1973**, *B11*, 33.

(22) Berry, G. C.; Fox, T. G. *Adv. Polym. Sci.* **1967**, *5*, 261.
(23) Barlow, A. J.; Erginsay, A.; Lamb, J. *Proc. R. Soc. London* **1967**, *298*, 481.
(24) Williams, G. *Trans. Faraday. Soc.* **1963**, *59*, 1397.
(25) Yin, T. P.; Ferry, J. D. *J. Colloid Sci.* **1961**, *16*, 166.
(26) Doolittle, A. K. *J. Appl. Phys.* **1951**, *22*, 1471.
(27) Ferry, J. D. *Viscoelastic Properties of Polymers*, 3rd ed.; John Wiley and Sons: New York, 1980.
(28) Chen, H. Y.; Stepanov, E. V.; Chum, S. P.; Hiltner, A.; Baer, E. *Macromolecules* **2000**, *33*, 8870.
(29) Hodge, I. M.; Eisenberg, A. *Macromolecules* **1978**, *11*, 283.
(30) Kannan, R. M.; Lodge, T. P. *Macromolecules* **1997**, *30*, 3694.
(31) Miller, A. A. *Macromolecules* **1978**, *11*, 859.
(32) Kovacs, A. *Adv. Polym. Sci.* **1964**, *3*, 394.
(33) Okubo, M.; Inoue, M.; Suzuki, T.; Kouda, M. *Colloid Polym. Sci.* **2004**, *282*, 1150.